PRIFYSGOL BANGOR / BANGOR UNIVERSITY

PRIFYSGOL
BANGOR
UNIVERSITY

Climatic Consequences of a Pine Island Glacier Collapse

Green, J.A.M.; Schmittner, A.

Journal of Climate

DOI:
10.1175/JCLI-D-15-0110.1
10.1175/JCLI-D-15-0110.1

Published: 07/12/2015

Publisher's PDF, also known as Version of record

Cyswllt i'r cyhoeddiad / Link to publication

Dyfyniad o'r fersiwn a gyhoeddwyd / Citation for published version (APA):
Green, J. A. M., & Schmittner, A. (2015). Climatic Consequences of a Pine Island Glacier Collapse. *Journal of Climate*, *28*(23), 9221-9234. https://doi.org/10.1175/JCLI-D-15-0110.1, https://doi.org/10.1175/JCLI-D-15-0110.1

Hawliau Cyffredinol / General rights
Copyright and moral rights for the publications made accessible in the public portal are retained by the authors and/or other copyright owners and it is a condition of accessing publications that users recognise and abide by the legal requirements associated with these rights.

• Users may download and print one copy of any publication from the public portal for the purpose of private study or research.
• You may not further distribute the material or use it for any profit-making activity or commercial gain
• You may freely distribute the URL identifying the publication in the public portal ?

Take down policy
If you believe that this document breaches copyright please contact us providing details, and we will remove access to the work immediately and investigate your claim.

05. May. 2023

Climatic Consequences of a Pine Island Glacier Collapse

J. A. M. GREEN

School of Ocean Sciences, Bangor University, Menai Bridge, United Kingdom

A. SCHMITTNER

College of Earth, Ocean and Atmosphere Sciences, Oregon State University, Corvallis, Oregon

(Manuscript received 6 February 2015, in final form 20 August 2015)

ABSTRACT

An intermediate-complexity climate model is used to simulate the impact of an accelerated Pine Island Glacier mass loss on the large-scale ocean circulation and climate. Simulations are performed for preindustrial conditions using hosing levels consistent with present-day observations of 3000 $m^3 s^{-1}$, at an accelerated rate of 6000 $m^3 s^{-1}$, and at a total collapse rate of 100 000 $m^3 s^{-1}$, and in all experiments the hosing lasted 100 years. It is shown that even a modest input of meltwater from the glacier can introduce an initial cooling over the upper part of the Southern Ocean due to increased stratification and ice cover, leading to a reduced upward heat flux from Circumpolar Deep Water. This causes global ocean heat content to increase and global surface air temperatures to decrease. The Atlantic meridional overturning circulation (AMOC) increases, presumably owing to changes in the density difference between Antarctic Intermediate Water and North Atlantic Deep Water. Simulations with a simultaneous hosing and increases of atmospheric CO_2 concentrations show smaller effects of the hosing on global surface air temperature and ocean heat content, which the authors attribute to the melting of Southern Ocean sea ice. The sensitivity of the AMOC to the hosing is also reduced as the warming by the atmosphere completely dominates the perturbations.

1. Introduction

The impact on the large-scale ocean circulation, and hence climate, by large inputs of freshwater or ice from collapsing ice sheets has been intensely studied in recent years [see Rahmstorf (2002) for a review]. The main climatic impact comes from the ability of the freshwater to hamper deep-water formation in the North Atlantic and thus reduce or even switch off the important Atlantic meridional overturning circulation (AMOC; see, e.g., Rahmstorf 2003; Green et al. 2009). Focus, however, has been on the deglaciation of the Northern Hemisphere ice sheets (e.g., Bigg et al. 2011), with fewer investigations looking at the impact of freshwater inputs from an Antarctic ice sheet collapse (Weaver et al. 2003; Hellmer 2004; Stouffer et al. 2007; Stammer 2008), from ice sheet collapses in either hemisphere (e.g., Hansen et al. 2015; note that they use very large hosing levels in their paper), or from melting sea ice (e.g., Aiken and England 2008). Recently, it was reported that Pine Island Glacier (PIG) in Antarctica has started a rapid retreat that has doubled the mass of ice being discharged annually from the glacier (Favier et al. 2014; McMillan et al. 2014; Rignot et al. 2014) and that it may continue to change rapidly over the next decades (Seroussi et al. 2014). Here we show, using a coupled Earth system model (Weaver et al. 2001), that even the modest increased input of freshwater from PIG can have a large-scale impact on the ocean and climate. This suggests that there may be important consequences of a collapsing Antarctic ice sheet beyond the more commonly reported contribution to sea level rise (e.g., Shepherd and Wingham 2007).

Simulations of hosing from Antarctica during meltwater pulse 1A (16 400 years before present) show a large impact on the ocean and climate (Weaver et al. 2003), including the interesting result that as the Southern Hemisphere cools the Northern Hemisphere,

Denotes Open Access content.

Corresponding author address: Dr. J. A. M. Green, School of Ocean Sciences, Bangor University, Askew St., Menai Bridge LL59 5AB, United Kingdom.
E-mail: m.green@bangor.ac.uk

DOI: 10.1175/JCLI-D-15-0110.1

© 2015 American Meteorological Society

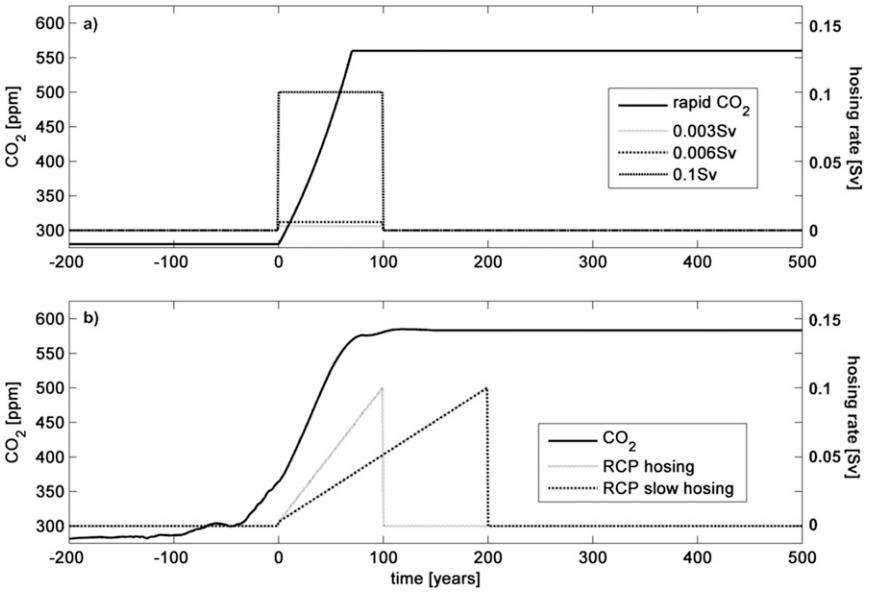

FIG. 1. (a) Time series of the hosing rates used in the preindustrial simulations and for the exponential CO_2 scenarios, along with the CO_2 concentration in the rapid CO_2 simulation (solid). Note that the hosing *y*-axis scale is to the right of the panel. (b) Time series of atmospheric CO_2 concentration (solid; scale to the left) and freshwater fluxes (dotted; scale to the right) used during the RCP scenarios. Note that model year 0 is equal to calendar year 2000 in the RCP scenarios; the axis has been shifted so that the hosing starts at year 0 in all scenarios (denoted "time" or "time from start" in the figures).

especially the North Atlantic, warms up. This bipolar seesaw in surface temperatures is caused by the reduction of density of the Antarctic Intermediate Water (AAIW) in the Southern Ocean, which leads to enhanced North Atlantic Deep Water (NADW) formation and hence an enhanced AMOC (Crowley 1992; Broecker 1998; Ganopolski and Rahmstorf 2001; Weaver et al. 2003; Saenko et al. 2003; Schmittner et al. 2003; Stocker and Johnsen 2003; Buizert et al. 2015). The associated heat transport northward increases, which has been found to cause the cooling of the Southern Ocean (Weaver et al. 2003).

PIG is a large ice stream discharging into Pine Island Bay in the Amundsen Sea, Antarctica. It drains some 10% of the West Antarctic Ice Sheet (WAIS; Shepherd et al. 2001; Payne et al. 2004; Vaughan et al. 2006), and recently it has been suggested that this drainage has increased over the last decades (Rignot et al. 2008; Rignot 2008; Wingham et al. 2009; Scott et al. 2009; Favier et al. 2014). Furthermore, the base of PIG lies below sea level on a retrograde slope, which means there is no topographic barrier to halt a retreat once it has been set in motion (Hughes 1981). Over the period 2003–14, West Antarctica has been losing ice mass at a rate of 121 Gt yr^{-1} (Harig and Simons 2015). Shepherd et al. (2012) reported a net discharge of 20 Gt yr^{-1} from PIG during the period 1992–2011, and Park et al. (2013) show that the retreat is accelerating. Projection by Favier et al. (2014) suggests that the mass loss will increase to 100 Gt annually around 2030 and may then remain constant (Favier et al. 2014). This accelerated retreat of PIG could have consequences for both regional and global ocean circulation patterns and climate and is the topic of this paper; specifically, we introduce relatively small levels of freshwater hosing in the Amundsen Sea in a coupled climate model of intermediate complexity. We will discuss three sets of experiments: sensitivity simulations with hosing during preindustrial conditions, idealized sensitivity simulations with hosing with rapid exponentially increasing atmospheric CO_2, and a set of more realistic simulations with more gradually changing atmospheric CO_2 levels and variable hosing.

2. Methods

Simulations were done with the University of Victoria Earth System Climate Model v2.8 (UVic ESCM; Weaver et al. 2001; Schmittner et al. 2008). The ocean component has a global configuration with 100 × 100 grid cells in the horizontal and 19 vertical layers. It is coupled to a simplified thermodynamic atmosphere that allows for exchange of heat and water vapor but without feedback to the prescribed wind field, which comes from repeating the mean annual cycle of monthly data from

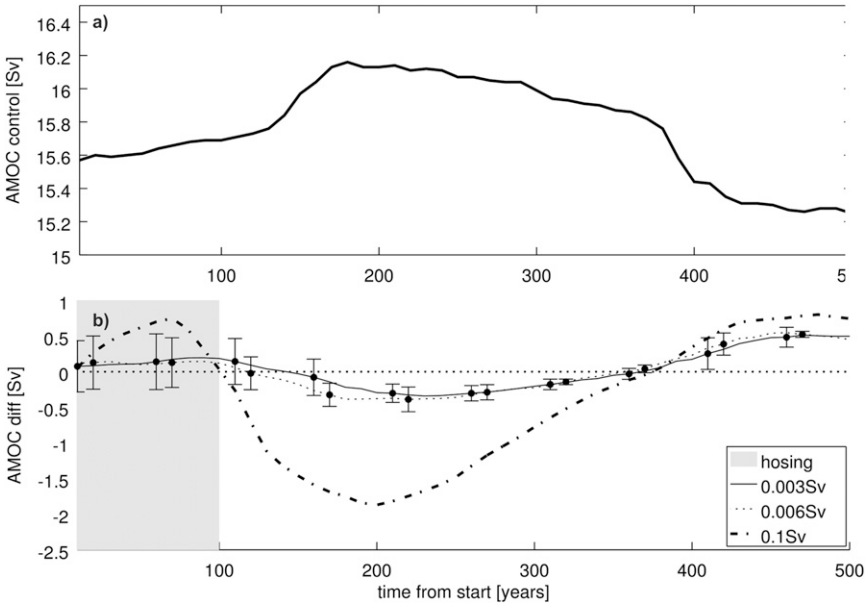

FIG. 2. (a) AMOC control at 26°N (in Sv), averaging at 15.6 Sv. (b) Difference between the preindustrial perturbation runs and the long-term average of the control plotted against time from start of the hosing perturbations. The hosing period is shaded in gray. The error bars every 50 years on the 0.003- (bold) and 0.006-Sv runs mark ±1 standard deviation of the ensemble data. Note that the bars are offset 10 years for clarity and that we use a different range, again for clarity, between the different AMOC figures.

the National Centers for Environmental Prediction (NCEP) reanalysis. The model also includes a dynamic and thermodynamic sea ice model and prescribed continental ice sheets.

The first series of sensitivity simulations were run for preindustrial conditions with orbital parameters set to those of the year 1800 and CO_2 levels at 280 ppm. These experiments included a 100-yr-long hosing of 0.003, 0.006, and 0.1 Sv ($1\,\text{Sv} = 10^6\,\text{m}^3\,\text{s}^{-1}$), respectively, and are compared to a control simulation without hosing (see Fig. 1a for a schematic). The simulations were then continued for a further 400 years after the hosing had ended to allow for an evaluation of the recovery after a hosing event. The 0.003-Sv hosing represents the projected situation for 2030 described in Favier et al. (2014), whereas the 0.1-Sv case represents a sensitivity simulation in which the entire volume of PIG is released over a 100-yr period (Vaughan et al. 2006), a case of extremely fast melting. The 0.006-Sv release case is an intermediate simulation assuming a doubling of the present-day rate, thus representing an accelerated situation to the present, but still ends within 100 years. The 100-yr period of hosing is quite conservative and assumes a rapid retreat followed by a new stable state. In all simulations the hosing water is added to the two coastal grid cells nearest to PIG and the volume flux is evenly divided between the grid cells in these experiments.

The AMOC was computed by integrating the meridional velocity zonally across the Atlantic basin along 26°N and vertically between 1000-m depth and the sea bed (looking at the maximum of the overturning streamfunction produces very similar results, which are not shown). From this, it is clear that the model's internal (unforced) variability, particularly on interannual to multidecadal time scales, is much smaller than in observations or more comprehensive climate models. However, the control simulation of the model version used here exhibits multicentennial internal AMOC variability of ~1 Sv (see Fig. 2, which is discussed in more detail later). To separate the forced signal, which is small in the preindustrial simulations, from this internal "noise," we performed an ensemble of five simulations with different initial conditions by staggered starting points for the hosing by 100 years over the 500-yr control period. Each perturbation scenario is presented as an average of these five perturbation simulations.

To test the sensitivity of the response of the Earth system to hosing in a warming world, atmospheric CO_2 was increased exponentially over 70 years from preindustrial levels, ending with a doubled CO_2 concentration in the atmosphere, which was then held constant until the end of the 500-yr simulation. Runs were also done with a 100-yr hosing at 0.003- or 0.1-Sv levels in combination with increasing CO_2. Note that because of

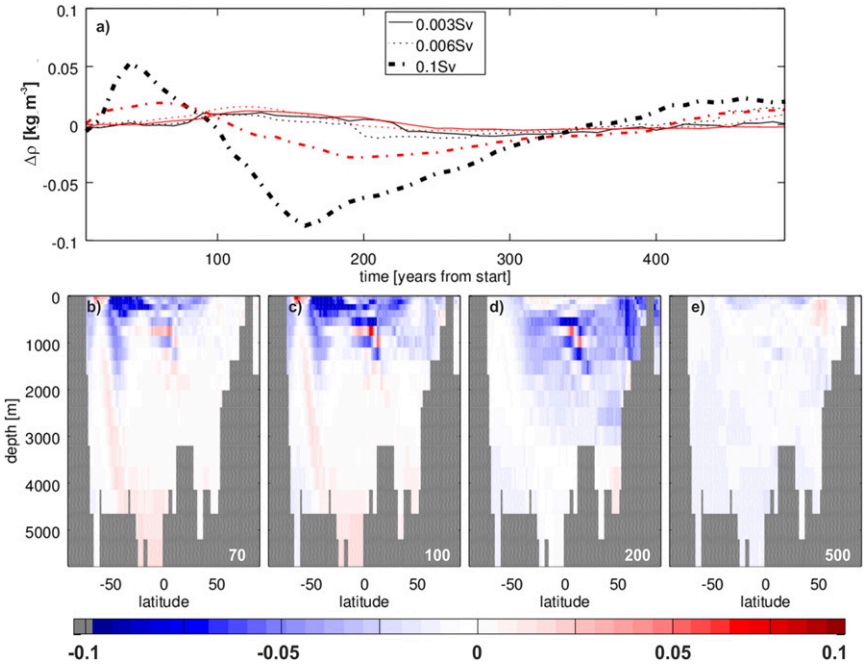

FIG. 3. (top) The time evolution of the density difference between the NADW and AAIW between the preindustrial perturbation runs and the control (red) and the density difference between the surface waters in the North Atlantic and Ross Sea (black). (bottom) The evolution (see numbers for time slices) of the density difference between the ensemble mean of the 0.1-Sv preindustrial run and the control along 20°W in the Atlantic.

the magnitude of the signals, we did not perform staggered restarts for the CO_2 scenarios.

The final set of simulations discussed uses a more realistic climate forcing, with CO_2 levels allowed to vary according to the representative concentration pathway 4.5 (RCP4.5) scenario (Meinshausen et al. 2011; Fig. 1b). This is an intermediate-level scenario, in which the greenhouse gas emissions stabilize around 2150. It was chosen over perhaps more-realistic larger emission scenarios because, as is shown below, large CO_2 increases dominate over the hosing signal. In these simulations, the model was restarted at calendar year 1800 and the simulation lasted for 700 years, with CO_2 evolving as in Fig. 1. These arguably more-realistic simulations with hosing were done by switching the hosing on at calendar year 2000 (i.e., model year 200) and allowing it to ramp up from 0.003 Sv at the start to 0.1 Sv at the end of the 100-yr hosing period (see Fig. 2). This corresponds to PIG losing half of its volume over 100 years. At that point the hosing abruptly switched off, simulating a retreating ice sheet that has suddenly reached a new stable state. A further simulation again started at a rate of 0.003 Sv and ramped up to 0.1 Sv over 200 years, after which it switched off (thus representing a total loss of the present-day PIG ice volume over 200 years). These simulations are referred to as "RCP control," "RCP hosing," and "RCP slow hosing," respectively.

3. Results

a. *Sensitivity simulations*

The preindustrial AMOC response to hosing behaves like a damped oscillator: it increases, drops down again, and then increases again toward the end of the simulation (Fig. 2). The initial increase and the subsequent decrease occur faster the stronger the forcing. The AMOC response is related to the NADW–AAIW density difference (see Fig. 3a, red lines, and the discussion below) and the density difference between the surface layers in both regions (black lines in Fig. 3a). In Fig. 3 we took the zonally averaged density across the Atlantic at 3200 m at 53°N to represent NADW and the zonally averaged density (again spanning the Atlantic) at 1100 m at 55°S to represent AAIW. The latter limits are based on a minimum in the control salinity in that region. The high correlation between the density differences and the perturbed AMOC strength confirms the suggested seesaw mechanism: we find correlation coefficients of 0.87, 0.78, and 0.95 at 99% confidence for the 0.003-, 0.006-, and 0.1-Sv simulations, respectively. The black lines in

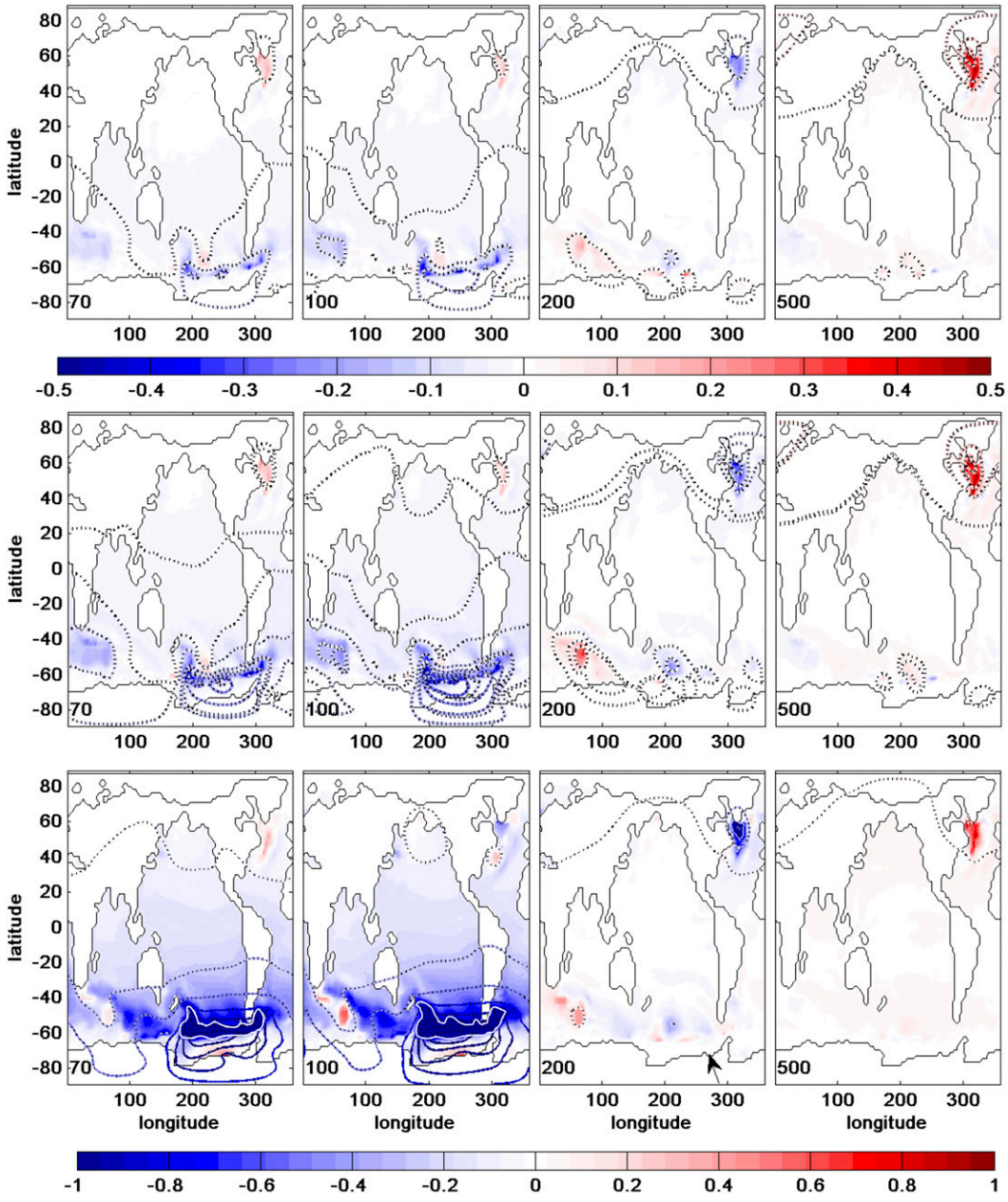

FIG. 4. The difference in sea surface temperature between the time-averaged control run and the ensembles for the sensitivity (top) 0.003-, (middle) 0.006-, and (bottom) 0.1-Sv simulations. The numbers in the lower left hand corner of each pane show the time in years from perturbation start and have been chosen for periods with large changes in the AMOC (cf. Fig. 2). Contoured in colored and dotted lines are the surface atmospheric differences using the same color scale [note the different scales between the top and middle panels and the bottom panel]. In the top and middle panels the isoline separation is 0.1°C, whereas in the bottom panel it is 0.2°C. The white ocean contour line for years 70 and 100 in the bottom panel mark −1°C change. The arrow in the 0.1-Sv scenario, year 200, marks the hosing location.

Fig. 3a were computed as the average density difference between the sea surface waters in an area spanning the North Atlantic between 55° and 65°N and the Atlantic sector of the Southern Ocean between the Antarctic coast and 64°S. The surface density difference appears to lead the deep density difference and AMOC changes.

The preindustrial 0.003- and 0.006-Sv runs show a quite large response to the hosing in both the ocean and atmosphere, especially considering the relatively small rate of freshwater addition (Fig. 4, top and middle), with an even larger signal in the 0.1-Sv run (Fig. 4, bottom). At the end of the pulse (i.e., at model year

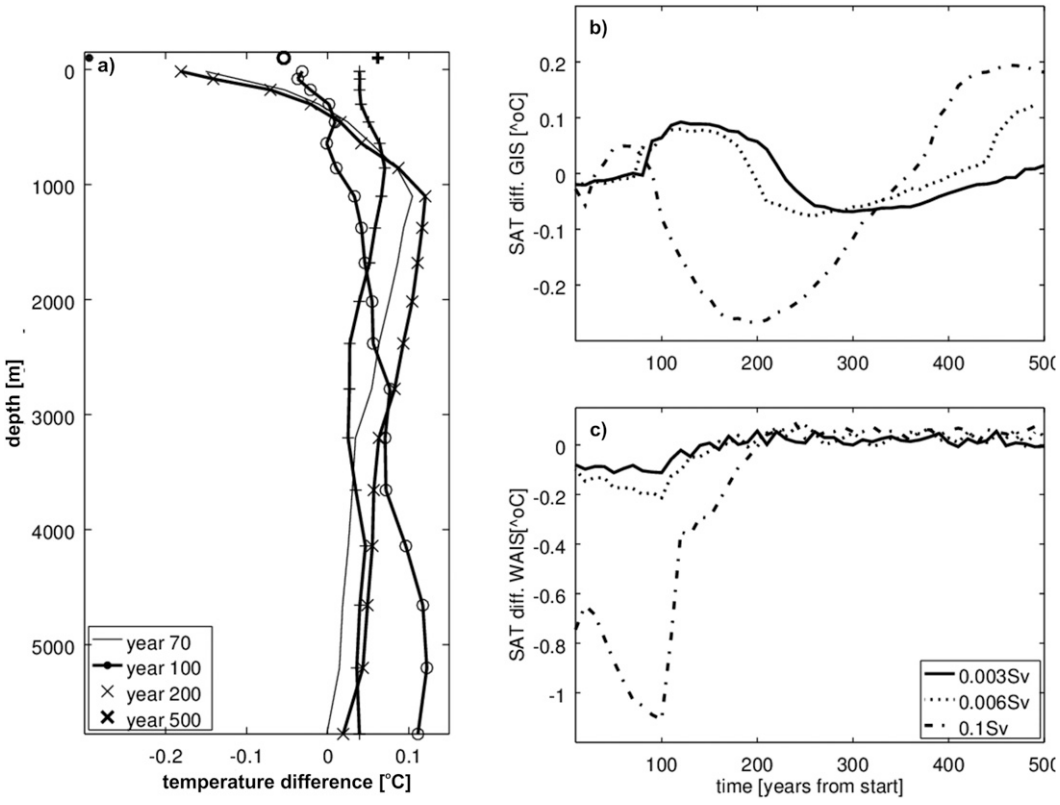

FIG. 5. (a) The globally averaged ocean temperature differences between the 0.1-Sv run and the time-averaged preindustrial control run as a function of depth. The various lines correspond to the time slices in Fig. 4. SAT difference between perturbation and control runs when spatially averaged over (b) the full extent of Greenland and (c) the full extent of WAIS. The panels again show the ensemble mean of the preindustrial runs. Note the varying *y*-axis scales in all the panels.

100), the sea surface temperature around parts of Antarctica, mainly in the Pacific sector of the Southern Ocean and in the Drake Passage, has dropped by up to 0.5°C in the 0.003- and 0.006-Sv simulations and substantially cooled over much of the Southern Ocean by over 1°C in the 0.1-Sv run (the white contour lines in Fig. 4 mark −1°C change). Differences between our Fig. 4 (bottom) and Figs. 4c,d in Weaver et al. (2003) are instructive. While the large differences between Figs. 2c and 4c,d in Weaver et al. (2003) indicate that the Southern Ocean cooling is strongly dependent on the location of the forcing, all their cases have an associated warming in the North Atlantic, which is consistent with their interpretation that the Southern Ocean cooling is caused by the bipolar seesaw mechanism (i.e., increased northward heat transport due to a stronger AMOC). In the present paper, however, there is only a weak warming over the first 50–100 years in the North Atlantic (less than 0.2°C around southern Greenland) but a relatively strong cooling (more than 1°C) in the Southern Ocean north of the Ross Sea (Fig. 4), which suggests that there is a local component at play besides the bipolar seesaw mechanism. The most likely candidate is that the upwelling of warmer water (Circumpolar Deep Water) has been prohibited by the meltwater acting as a lid on the ocean, consistent with Stouffer et al. (2007). Parts of the Southern Ocean have experienced a warming at year 200 with a corresponding cooling in the North Atlantic. Subsequently, toward the end of the simulation, the North Atlantic warms. The globally averaged sea surface and surface atmospheric temperatures at the same time have decreased by 0.2° and 0.35°C, respectively, in the 0.1-Sv case (Fig. 5a).

The driver of the temperature response in the North Atlantic seen in Figs. 4 and 5b is AMOC variability triggered by the freshwater perturbation in the Southern Ocean. The mechanism may be related to the bipolar seesaw and the associated change in density difference between the NADW and the AAIW, which has been suggested to influence NADW formation (Fig. 3; see also Weaver et al. 2003; Schmittner et al. 2003; Stouffer

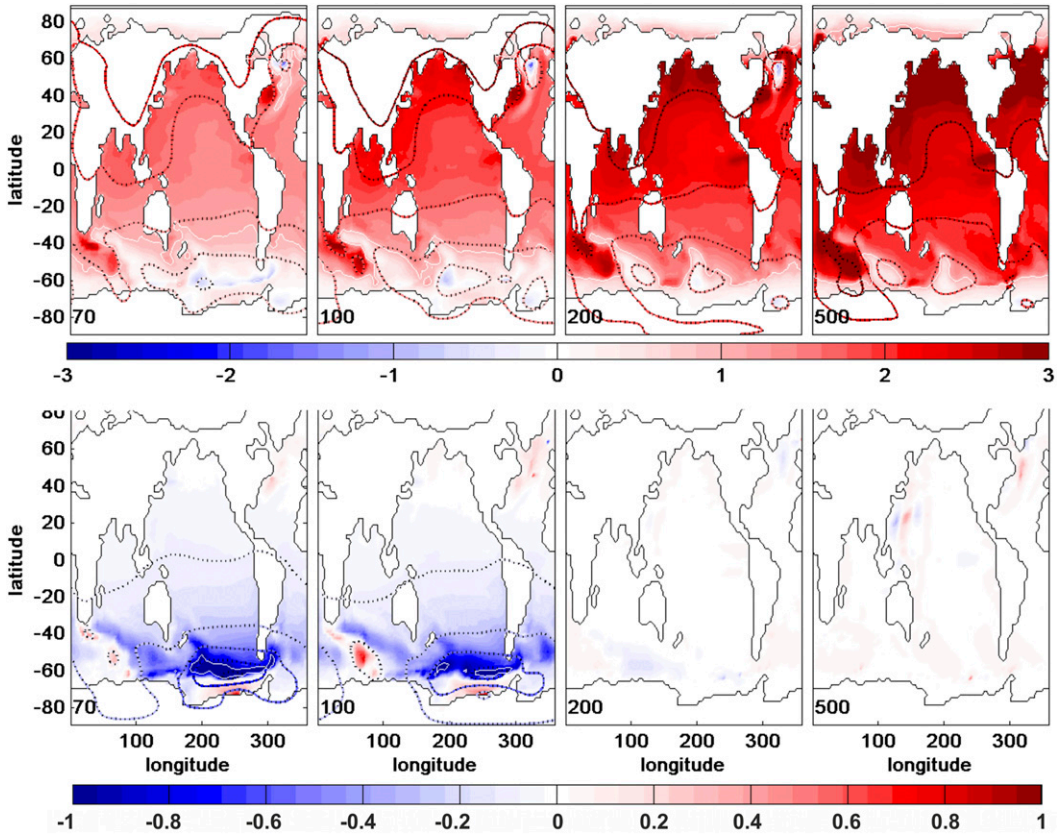

FIG. 6. (top) The differences between the rapid CO_2 and the preindustrial control in sea surface temperature (colors) and surface atmospheric temperature (contours). (bottom) The 0.1-Sv rapid CO_2 simulation minus the CO_2 control. Note the different color scales used in this figure. The contour interval for the atmospheric temperature is 0.5°C in the top panel and 0.2°C in the bottom.

et al. 2007). However, the enhanced AMOC seen in Fig. 2 and the changes in vertical stratification in the Atlantic in Fig. 3 then swing the seesaw the other way, leading to a strong cooling in the North Atlantic around year 200 in all the runs. Toward the end of the simulation the seesaw is back in a North Atlantic warming state (Fig. 4), but the full extent of the warming in the 0.1-Sv scenario is delayed until the end of the simulation. These changes in the ocean temperature drive corresponding changes in the atmosphere's surface temperature (Fig. 4, contours), with peak anomalies passing 1°C cooling in the 0.1-Sv sensitivity simulation.

Closer to the Antarctic coastline, there is initially a warming of up to 0.5°C near PIG and under the Ross ice shelf in the 0.1-Sv scenario (Fig. 4, bottom), which may lead to further acceleration of the ice loss. This warming is due to the meltwater creating a shallower surface mixed layer there, which can heat up more easily during the summer months when the area is free from sea ice; the sea ice may then act as insulation over the winter months for this water (note that the cooling discussed in the previous paragraph takes place offshore from the area under discussion here). Over the region offshore from PIG there is a net heat uptake relative to the control by the ocean (not shown) of up to 10 W m^{-2} during the first 150 years, followed by a declining heat loss until there is no significant net heat flux at year 500. No discernible effects were seen under the Filchner–Ronne ice shelf in our simulations, but the general trend over the Southern Ocean is for a cooling of the upper ocean and the atmosphere. This may impact ice shelf cavity waters (e.g., Fer et al. 2012), but we are not able at this stage to say what the impact will be.

b. *Rapid CO_2 simulations*

In the rapid CO_2 simulations the upper part of the ocean warms 2°–5°C in both the control and 0.1-Sv simulations (see Figs. 6–7). However, the relatively large response to the hosing seen in the preindustrial ocean and atmosphere is not reproduced in the rapid CO_2 simulations (see, e.g., Fig. 8 for the AMOC

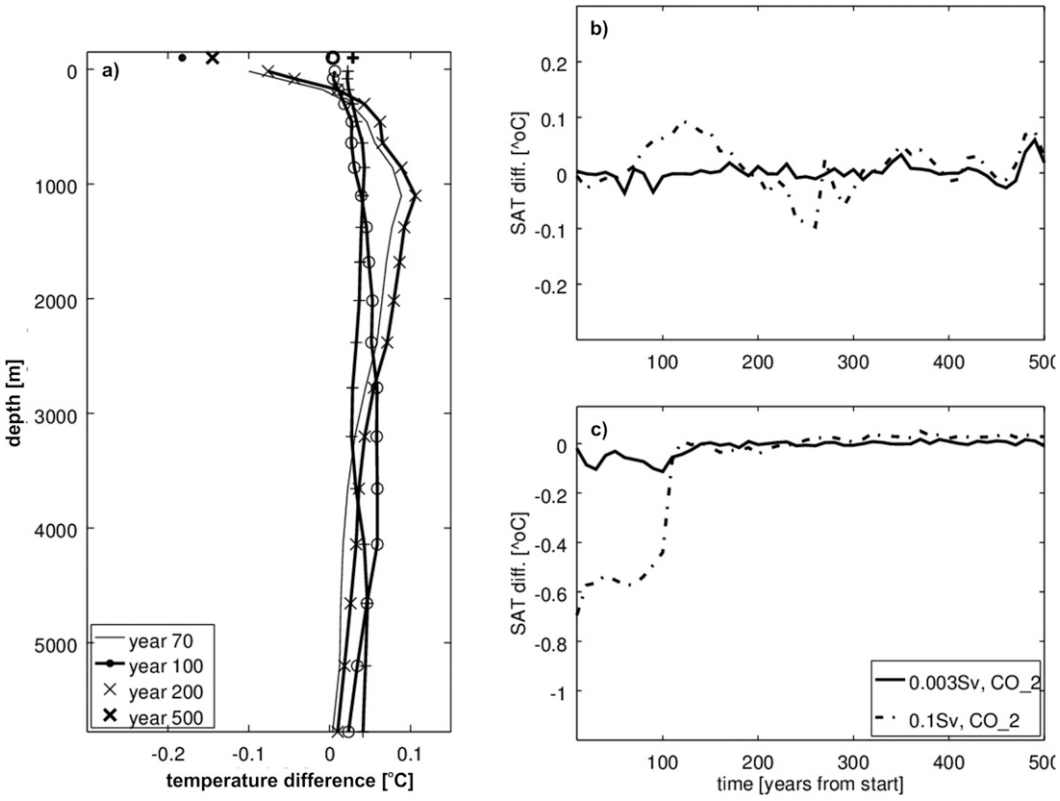

FIG. 7. As in Fig. 5, but for the rapid CO_2 simulation being compared to the rapid CO_2 control.

response). In the rapid CO_2 simulations, the 0.003-Sv forcing has a much smaller impact than in the preindustrial runs, suggesting that the CO_2 forcing is so large that any additional small hosing will not have an effect. The heating of the ocean and atmosphere has a profound impact on the AMOC, which drops by 6.5 Sv within 100 years of the start of the run because of the prevention of deep-water formation in the North Atlantic (Fig. 8). However, the AMOC rapidly recovers when the CO_2 has plateaued at year 70. This is despite the warmer surface ocean, as the interior of the Atlantic starts to fill up with new deep water from both the North Atlantic and the Southern Ocean, which resets the density difference between the NADW and AAIW (Fig. 9). In contrast to the CO_2 0.003-Sv hosing experiment, which has virtually no impact on the AMOC, the 0.1-Sv run does impact the AMOC, but it shows interesting differences from the preindustrial simulations. In the rapid CO_2 0.1-Sv run the cooling is weaker near the hosing area at year 100 (see Figs. 4 and 6), whereas there is more cooling in the Northern Hemisphere and North Atlantic compared to the preindustrial 0.1-Sv run (see the synthesis section below, and figures referred to there, where we argue that this is because of changes in Southern Ocean ice cover). The horizontally averaged ocean temperatures increase (Fig. 7a), indicating that the excess heat is stored in the ocean. Over Greenland the hosing has only a small effect on the response of the atmospheric temperature compared to the CO_2 control run (Fig. 7b), whereas over the WAIS the larger hosing acts to delay the atmospheric warming as a result of a brief cooling of the Southern Ocean (compared to the CO_2 control; Fig. 7c).

c. *RCP4.5 simulations*

The RCP AMOC initially reduces by about 5 Sv when the atmospheric CO_2 rapidly increases (Fig. 10). It then recovers to preindustrial levels once the CO_2 stabilizes at 580 ppm. The RCP control (Fig. 11, top) shows a global warming of the atmosphere exceeding 5°C on average at year 350 compared to the preindustrial control, whereas the ocean surface warms more than 3.5°C on average (Fig. 11, top). The hosing simulations, when compared to the RCP control in Fig. 11, indicate the same type of signal we have seen in the idealized rapid CO_2 runs but at a somewhat weaker magnitude compared to the sensitivity simulations (Fig. 11, middle). As could be expected, the effect of the hosing is more pronounced in the faster hosing experiment during the first 100 years (Fig. 11, middle

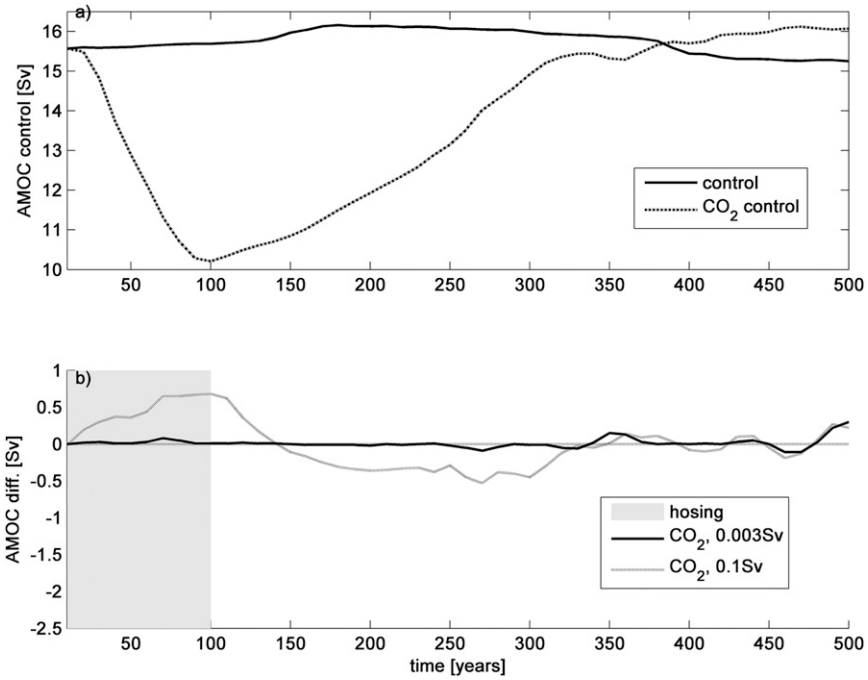

FIG. 8. As in Fig. 2, but for the rapid CO_2 simulations. The differences in (b) are deviations from the CO_2 control [dotted line in (a)].

and bottom), but the effects on the ocean are of course seen for a longer duration in the slow hosing. There are indications in the time-varying hosing runs of a bipolar seesaw acting on top of the warming in these simulations (e.g., Fig. 10, years 300 and 350), but compared to preindustrial levels it is surpassed by the warming from the increased atmospheric CO_2, just as in the rapid CO_2 simulations.

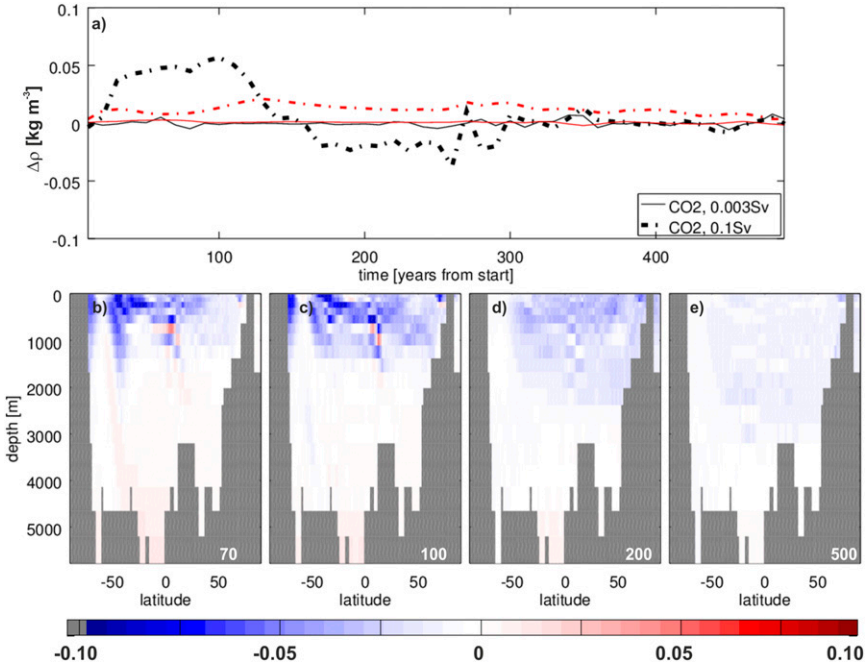

FIG. 9. As in Fig. 3, but for the rapid CO_2 perturbation compared to the rapid CO_2 control.

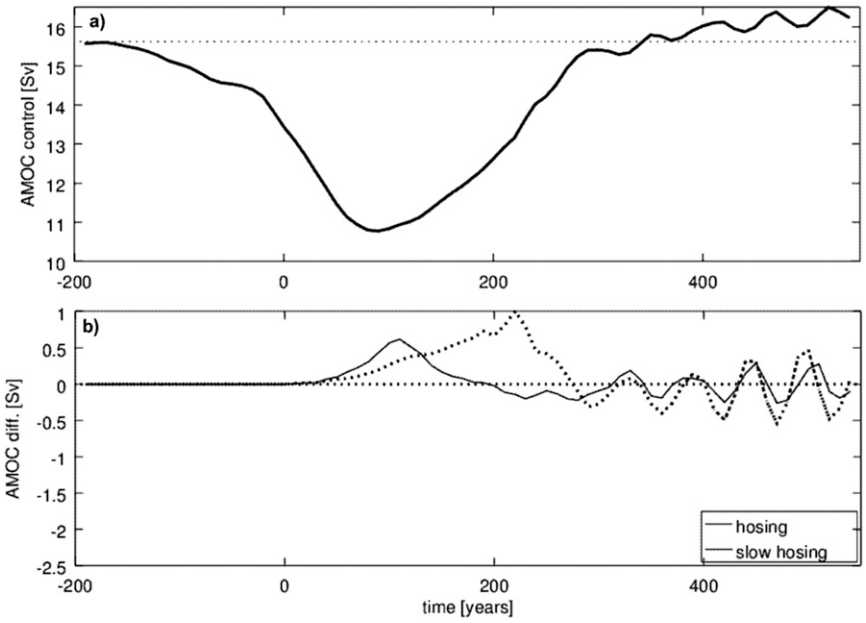

FIG. 10. As in Fig. 8, but for the RCP simulations. In (a) the thin dotted line marks the preindustrial control average, whereas (b) shows the RCP perturbations minus the RCP control. Note that the hosing starts at year 0 (see Fig. 1).

d. Synthesis

The hosing in all simulations leads to an increased ocean heat content, which leads to a subsequent atmospheric cooling (Fig. 12). One possible mechanism for the increase in oceanic heat is that the increased stratification and ice cover in the Southern Ocean prevents heat loss from the Circumpolar Deep Water. In the rapid CO_2 run this effect is smaller than in the preindustrial run. In the RCP run the heat content difference (compared to the RCP control) is even lower than the rapid CO_2 run (compared to the rapid CO_2 control), although the atmospheric cooling is, on average, at the same level (Fig. 12). Furthermore, there are larger differences in vertically integrated heat content at the end of the hosing periods near the ice edge in the Southern Ocean (Fig. 12, bottom). These differences are probably due to a smaller increase in the sea ice cover in the Southern Ocean in the CO_2 and RCP runs than in the PI run (see Fig. 13; note that in both simulations the sea ice area is larger than in their respective controls). Also, the extent of the ice cover in the Southern Ocean does not change much between the perturbation runs and their controls, but the ice area fraction does (not shown). This, together with the results in Fig. 13, implies that the perturbation runs have more and thicker ice in the regions that are ice covered in the control runs, which may prevent oceanic heat loss in the Southern Ocean. We therefore argue here that the sea ice melting in the rapid CO_2 and RCP runs is the cause of the weaker response of ocean heat content and atmospheric temperatures to the hosing.

The oceanic response, described by the AMOC, and sea surface and surface atmospheric temperatures evolve quite differently between the runs (see, e.g., Figs. 4–7). The robust features are the initial cooling of the Southern Ocean and the initial AMOC increase. The subsequent decrease seen in the preindustrial runs, however, is much smaller in the rapid CO_2 simulations and absent in the RCP run. The temperatures in the North Atlantic do not differ much between the preindustrial and the RCP runs, except for strong cooling in the rapid CO_2 runs around years 70–100.

4. Discussion

A bipolar seesaw has been found in the twentieth-century instrument record (Chylek et al. 2010), and we present further support for the seesaw being possible in present and future hosing scenarios. There is warming over Greenland seen during at least some stage in all the simulations, and the ocean initially warms in all runs. This may lead to an enhanced Greenland melting, which could eventually counteract the changes seen here by slowing down the AMOC, warming the Southern Ocean, and resetting the system. This would of course be on top of already accelerated losses of Greenland ice

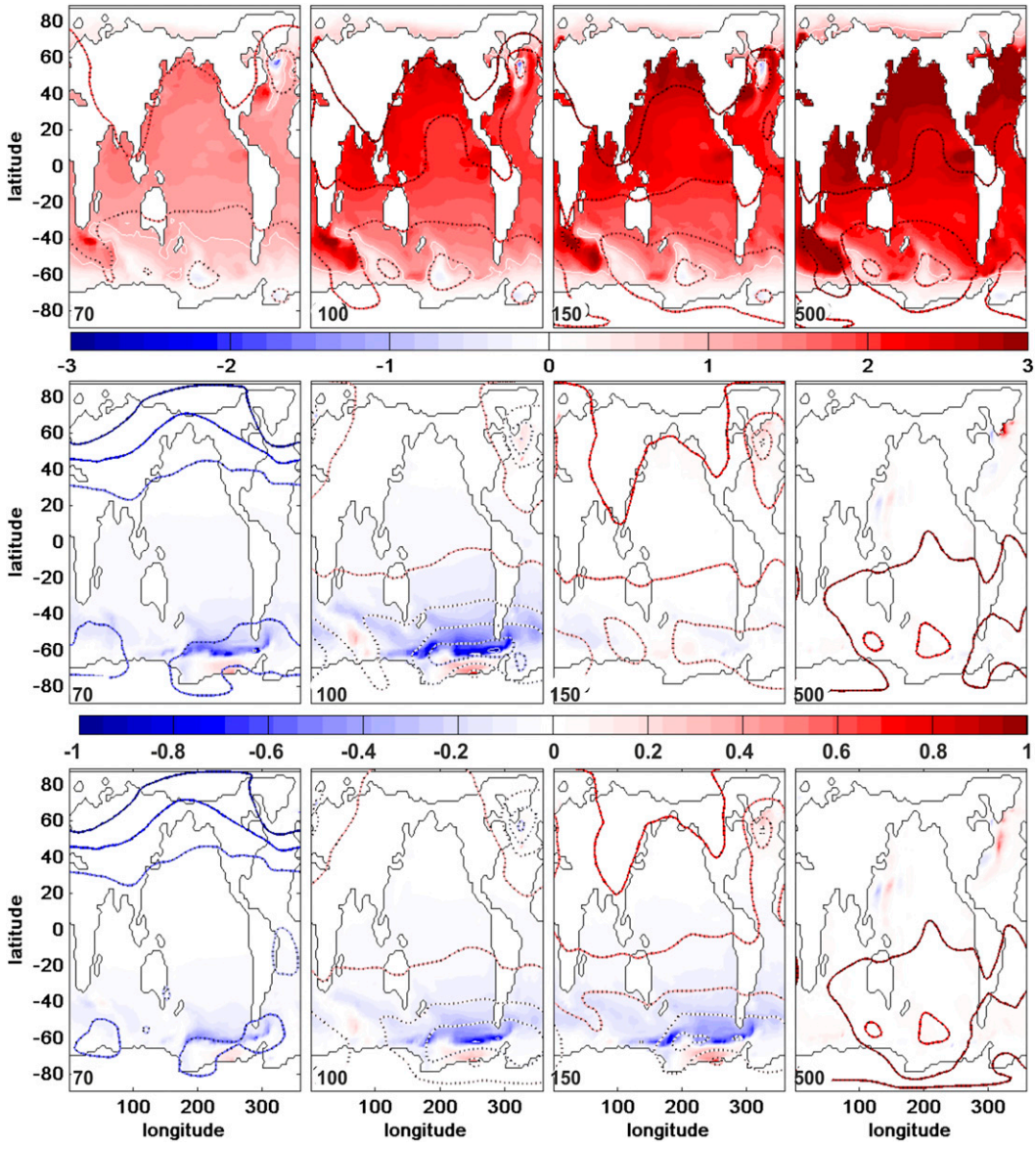

FIG. 11. As in Fig. 6, but for the RCP simulations. (middle) RCP hosing (over 100 years); (bottom) slow hosing (over 200 years). The atmospheric contour lines span −3°–3°C in intervals of 0.5°C (top) and −1 to 1°C in intervals of 0.2°C (middle),(bottom). Also, note the different color scales between the top and the bottom two panels. The timings are again as in Fig. 1, with the hosing starting at year 0.

due to warming over the last few decades (e.g., Steig et al. 2009; Nghiem et al. 2012; Ewert et al. 2012; Hanna et al. 2013). This highlights the importance of the neglected subject of climatic impacts of collapsing Antarctic ice sheets.

As a sensitivity simulation 0.003 Sv was added over the entire Southern Ocean rather than just off the coast of PIG. The response is very similar to that of the PIG 0.003-Sv scenario, although the amplitudes of the perturbations are somewhat reduced (not shown). This is also true for runs with 0.003 Sv added over the western or eastern half of the Antarctic Circumpolar Current (ACC; not shown). A further simulation was hosed with 0.05 Sv for 200 years, thus inputting the same amount of freshwater as the 0.1-Sv simulation. Again, the response is as expected, with a weaker signal than in the 0.1-Sv run but persisting throughout the 200-yr hosing. The insensitivity to the hosing location in both space and time is comforting and suggests that the results are robust.

UVic uses a simplified atmospheric model in which winds and cloud cover are prescribed. In the large-perturbation

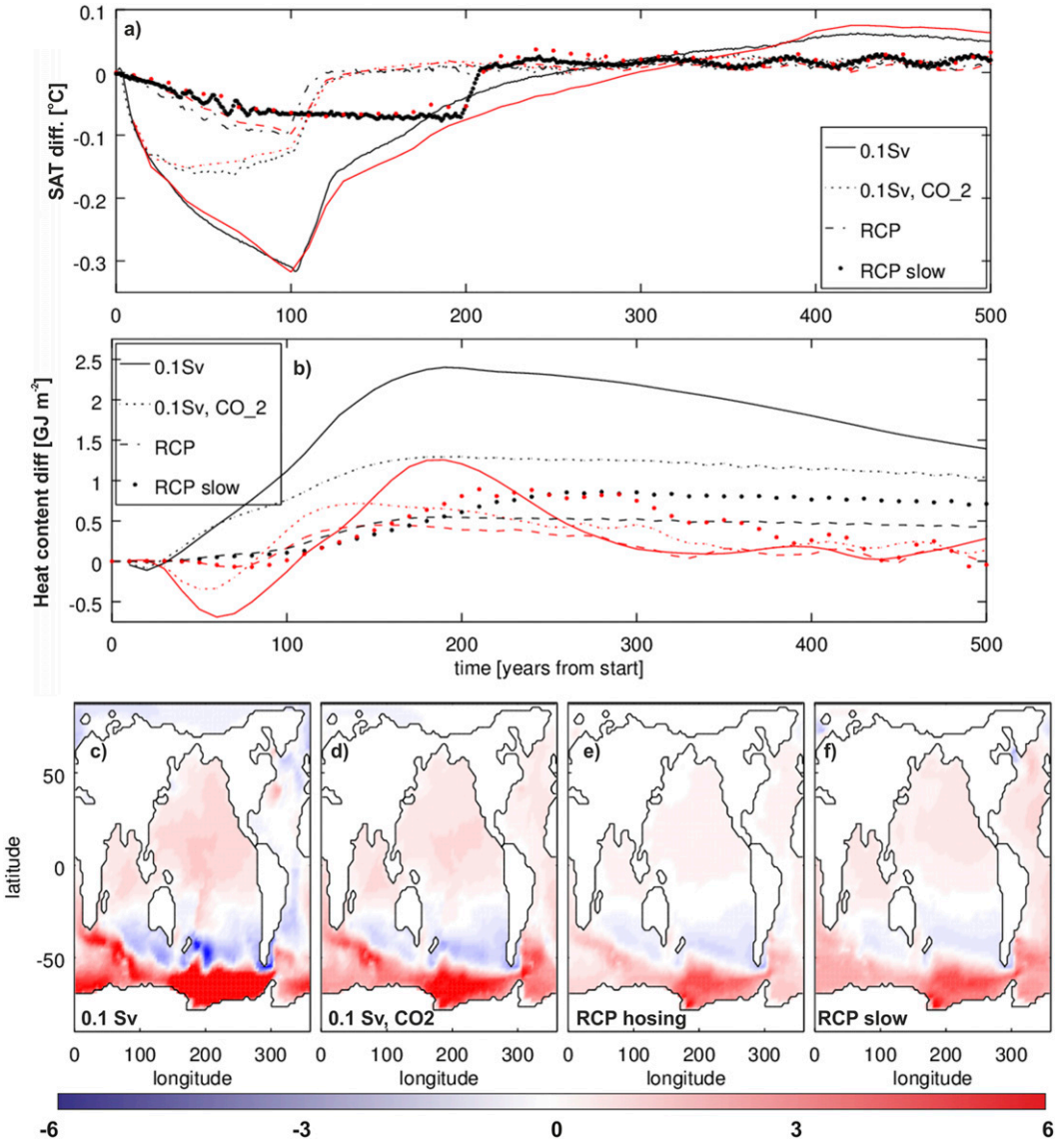

FIG. 12. Horizontal averages of (a) SAT and (b) vertically integrated heat content. Shown are differences between the 0.1-Sv perturbation runs and their respective controls and between the RCP hosing run and the RCP control. Black lines mark global averages, and red lines mark averages over the Atlantic only, between 60°S and 65°N. Depth-integrated heat content in GJ m^{-2} at the end of the hosing for the (c) 0.1-Sv hosing (data shown are from year 100), (d) rapid CO_2 0.1-Sv hosing (year 100), (e) RCP hosing (year 100), and (f) RCP slow hosing (year 200).

scenario and in the CO_2 simulations one would expect these parameters to change. Also, the model does not simulate weather, and its internal variability on interannual to decadal time scales is much smaller than observed. However, the model has been successfully used several times to simulate ocean states and climates different from the one of today [see Schmittner et al. (2008) for a discussion]; we argue that the simulations are a good first representation of potential consequences of a PIG collapse on ocean circulation but that it would be desirable to repeat the simulations with more comprehensive models.

We have shown that a spatially limited input of freshwater from Antarctica can impact the present and future large-scale ocean circulation and climate. The 0.003-Sv simulation represents a present collapse rate, whereas the 0.1-Sv run represents an upper-limit estimate. Qualitatively, our results are similar to those reported for meltwater pulse 1A (Weaver et al. 2003), which were suggested to trigger collapses of the

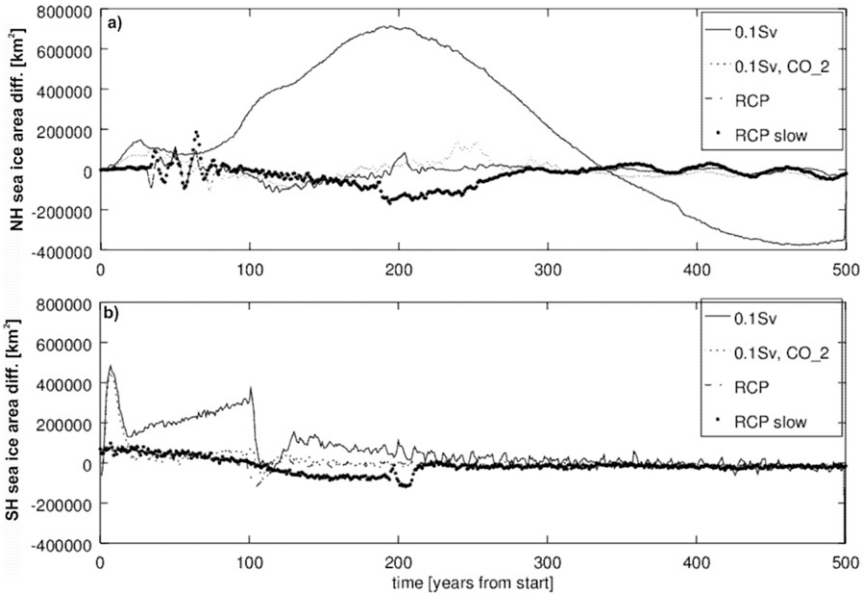

FIG. 13. The difference in (a) Northern and (b) Southern Hemisphere sea ice cover between perturbation and control runs.

Northern Hemisphere ice sheets during the deglaciation. Although the perturbations in atmospheric temperature are too small and too brief to generate large changes in the ice sheet extent, we suggest that a larger pulse than those used here (e.g., by other ice streams discharging as well) may indeed have profound impacts on other parts of the Earth system far away from PIG itself.

Acknowledgments. JAMG acknowledges funding from the Climate Change Consortium for Wales and from the Natural Environmental Research Council (Grant NE/F014821/1). AS is supported by grants from the National Science Foundation and the National Oceanic and Atmospheric Administration (Grant NA13OAR4310133). Comments from two anonymous reviewers and from the editor, Oleg Saenko, greatly improved the paper.

REFERENCES

Aiken, C. M., and M. H. England, 2008: Sensitivity of the present-day climate to freshwater forcing associated with Antarctic sea ice loss. *J. Climate*, **21**, 3936–3946, doi:10.1175/2007JCLI1901.1.

Bigg, G. R., R. C. Levine, and C. L. Green, 2011: Modelling abrupt glacial North Atlantic freshening: Rates of change and their implications for Heinrich events. *Global Planet. Change*, **79**, 176–192, doi:10.1016/j.gloplacha.2010.11.001.

Broecker, W. S., 1998: Paleocean circulation during the last deglaciation: A bipolar seesaw? *Paleoceanography*, **13**, 119–121, doi:10.1029/97PA03707.

Buizert, C., and Coauthors, 2015: Precise interpolar phasing of abrupt climate change during the last ice age. *Nature*, **520**, 661–665, doi:10.1038/nature14401.

Chylek, P., C. K. Folland, G. Lesins, and M. K. Dubey, 2010: Twentieth century bipolar seesaw of the Arctic and Antarctic surface air temperatures. *Geophys. Res. Lett.*, **37**, L08703, doi:10.1029/2010GL042793.

Crowley, T. J., 1992: North Atlantic deep water cools the Southern Hemisphere. *Paleoceanography*, **7**, 489–497, doi:10.1029/92PA01058.

Ewert, H., A. Groh, and R. Dietrich, 2012: Volume and mass changes of the Greenland ice sheet inferred from ICESat and GRACE. *J. Geodyn.*, **59**, 111–123, doi:10.1016/j.jog.2011.06.003.

Favier, L., and Coauthors, 2014: Retreat of Pine Island Glacier controlled by marine ice-sheet instability. *Nat. Climate Change*, **4**, 117–121, doi:10.1038/nclimate2094.

Fer, I., K. Makinson, and K. W. Nicholls, 2012: Observations of thermohaline convection adjacent to Brunt ice shelf. *J. Phys. Oceanogr.*, **42**, 502–508, doi:10.1175/JPO-D-11-0211.1.

Ganopolski, A., and S. Rahmstorf, 2001: Rapid changes of glacial climate simulated in a coupled climate model. *Nature*, **409**, 153–158, doi:10.1038/35051500.

Green, J. A. M., C. L. Green, G. R. Bigg, T. P. Rippeth, J. D. Scourse, and K. Uehara, 2009: Tidal mixing and the meridional overturning circulation from the last glacial maximum. *Geophys. Res. Lett.*, **36**, L15603, doi:10.1029/2009GL039309.

Hanna, E., and Coauthors, 2013: Ice-sheet mass balance and climate change. *Nature*, **498**, 51–59, doi:10.1038/nature12238.

Hansen, J., and Coauthors, 2015: Ice melt, sea level rise and superstorms: Evidence from paleoclimate data, climate modeling, and modern observations that 2°C global warming is highly dangerous. *Atmos. Chem. Phys. Discuss.*, **15**, 20 059–20 179, doi:10.5194/acpd-15-20059-2015.

Harig, C., and F. J. Simons, 2015: Accelerated West Antarctic ice mass loss continues to outpace East Antarctic gains. *Earth Planet. Sci. Lett.*, **415**, 134–141, doi:10.1016/j.epsl.2015.01.029.

Hellmer, H. H., 2004: Impact of Antarctic ice shelf basal melting on sea ice and deep ocean properties. *Geophys. Res. Lett.*, **31**, L10307, doi:10.1029/2004GL019506.

Hughes, T., 1981: The weak underbelly of the West Antarctic ice sheet. *J. Glaciol.*, **27**, 518–525.

McMillan, M., A. Shepherd, A. Sundal, K. Briggs, A. Muir, A. Ridout, A. Hogg, and D. Wingham, 2014: Increased ice losses from Antarctica detected by CryoSat-2. *Geophys. Res. Lett.*, **41**, 3899–3905, doi:10.1002/2014GL060111.

Meinshausen, M., and Coauthors, 2011: The RCP greenhouse gas concentrations and their extension from 1765 to 2300. *Climatic Change*, **109**, 213–241, doi:10.1007/s10584-011-0156-z.

Nghiem, S. V., and Coauthors, 2012: The extreme melt across the Greenland ice sheet in 2012. *Geophys. Res. Lett.*, **39**, L20502, doi:10.1029/2012GL053611.

Park, J. W., N. Gourmelen, A. Shepherd, S. W. Kim, D. G. Vaughan, and D. J. Wingham, 2013: Sustained retreat of the Pine Island Glacier. *Geophys. Res. Lett.*, **40**, 2137–2142, doi:10.1002/grl.50379.

Payne, A. J., A. Vieli, A. P. Shepherd, D. Wingham, and E. Rignot, 2004: Recent dramatic thinning of largest West Antarctic ice stream triggered by oceans. *Geophys. Res. Lett.*, **31**, L23401, doi:10.1029/2004GL021284.

Rahmstorf, S., 2002: Ocean circulation and climate during the past 120 000 years. *Nature*, **419**, 207–214, doi:10.1038/nature01090.

——, 2003: Thermohaline circulation: The current climate. *Nature*, **421**, 699, doi:10.1038/421699a.

Rignot, E., 2008: Changes in West Antarctic ice stream dynamics observed with ALOS PALSAR data. *Geophys. Res. Lett.*, **35**, L12505, doi:10.1029/2008GL033365.

——, J. L. Bamber, M. R. Van Den Broeke, C. Davis, Y. Li, W. J. Van De Berg, and E. Van Meijgaard, 2008: Recent Antarctic ice mass loss from radar interferometry and regional climate modelling. *Nat. Geosci.*, **1**, 106–110, doi:10.1038/ngeo102.

——, J. Mouginot, M. Morlighem, H. Seroussi, and B. Scheuchl, 2014: Widespread, rapid grounding line retreat of Pine Island, Thwaites, Smith, and Kohler glaciers, West Antarctica, from 1992 to 2011. *Geophys. Res. Lett.*, **41**, 3502–3509, doi:10.1002/2014GL060140.

Saenko, O. A., A. J. Weaver, and A. Schmittner, 2003: Atlantic deep circulation controlled by freshening in the Southern Ocean. *Geophys. Res. Lett.*, **30**, 1754, doi:10.1029/2003GL017681.

Schmittner, A., O. A. Saenko, and A. J. Weaver, 2003: Coupling of the hemispheres in observations and simulations of glacial climate change. *Quat. Sci. Rev.*, **22**, 659–671, doi:10.1016/S0277-3791(02)00184-1.

——, A. Oschlies, H. D. Matthews, and E. D. Galbraith, 2008: Future changes in climate, ocean circulation, ecosystems, and biogeochemical cycling simulated for a business-as-usual CO_2 emission scenario until year 4000 AD. *Global Biogeochem. Cycles*, **22**, GB1013, doi:10.1029/2007GB002953.

Scott, J. B. T., G. H. Gudmundsson, A. M. Smith, R. G. Bingham, H. D. Pritchard, and D. G. Vaughan, 2009: Increased rate of acceleration on Pine Island Glacier strongly coupled to changes in gravitational driving stress. *Cryosphere*, **3**, 125–131, doi:10.5194/tc-3-125-2009.

Seroussi, H., M. Morlighem, E. Rignot, J. Mouginot, E. Larour, M. Schodlok, and A. Khazendar, 2014: Sensitivity of the dynamics of Pine Island Glacier, West Antarctica, to climate forcing for the next 50 years. *Cryosphere*, **8**, 1699–1710, doi:10.5194/tc-8-1699-2014.

Shepherd, A., and D. Wingham, 2007: Recent sea-level contributions of the Antarctic and Greenland ice sheets. *Science*, **315**, 1529–1532, doi:10.1126/science.1136776.

——, ——, J. A. D. Mansley, and H. F. J. Corr, 2001: Inland thinning of Pine Island Glacier, West Antarctica. *Science*, **291**, 862–864, doi:10.1126/science.291.5505.862.

——, and Coauthors, 2012: A reconciled estimate of ice-sheet mass balance. *Science*, **338**, 1183–1189, doi:10.1126/science.1228102.

Stammer, D., 2008: Response of the global ocean to Greenland and Antarctic ice melting. *J. Geophys. Res.*, **113**, C06022, doi:10.1029/2006JC004079.

Steig, E. J., D. P. Schneider, S. D. Rutherford, M. E. Mann, J. C. Comiso, and D. T. Shindell, 2009: Warming of the Antarctic ice-sheet surface since the 1957 International Geophysical Year. *Nature*, **457**, 459–464, doi:10.1038/nature07669.

Stocker, T. F., and S. J. Johnsen, 2003: A minimum thermodynamic model for the bipolar seesaw. *Paleoceanography*, **18**, 1087, doi:10.1029/2003PA000920.

Stouffer, R. J., D. Seidov, and B. J. Haupt, 2007: Climate response to external sources of freshwater: North Atlantic versus the Southern Ocean. *J. Climate*, **20**, 436–448, doi:10.1175/JCLI4015.1.

Vaughan, D. G., and Coauthors, 2006: New boundary conditions for the West Antarctic ice sheet: Subglacial topography beneath Pine Island Glacier. *Geophys. Res. Lett.*, **33**, L09501, doi:10.1029/2005GL025588.

Weaver, A. J., and Coauthors, 2001: The UVic Earth System Climate Model: Model description, climatology, and application to past, present and future climates. *Atmos.–Ocean*, **39**, 361–428, doi:10.1080/07055900.2001.9649686.

——, O. A. Saenko, P. U. Clark, and J. X. Mitrovica, 2003: Meltwater pulse 1A from Antarctica as a trigger of the Bølling-Allerød warm interval. *Science*, **299**, 1709–1713, doi:10.1126/science.1081002.

Wingham, D. J., D. W. Wallis, and A. Shepherd, 2009: Spatial and temporal evolution of Pine Island Glacier thinning, 1995–2006. *Geophys. Res. Lett.*, **36**, L17501, doi:10.1029/2009GL039126.